

PAPER • OPEN ACCESS

## Investigation of the protection effect of ginger, tea tree and grapefruit essential oil extracts on mild steel in 0.5M H<sub>2</sub>SO<sub>4</sub> solution

To cite this article: Roland Tolulope Loto 2022 *Mater. Res. Express* 9 066509

View the [article online](#) for updates and enhancements.

You may also like

- [Norovirus-like VP1 particles exhibit isolate dependent stability profiles](#)  
Ronja Pogan, Carola Schneider, Rudolph Reimer et al.
- [Design optimization of broadband extreme ultraviolet polarizer in high-dimensional objective space](#)  
Shang-Qi Kuang, , Bo-Chao Li et al.
- [Evaluation of physical properties of enamel after microabrasion, polishing, and storage in artificial saliva](#)  
L S M Fragoso, D A N L Lima, R S de Alexandre et al.



**EDINBURGH INSTRUMENTS**

WORLD LEADING MOLECULAR SPECTROSCOPY SOLUTIONS

edinst.com

The advertisement features a red background with the Edinburgh Instruments logo on the left, which consists of a circular pattern of white dots. To the right, several pieces of laboratory equipment are displayed, including a spectrophotometer labeled 'F55', a larger instrument labeled 'FLS 1000', and a microscope. The text 'WORLD LEADING MOLECULAR SPECTROSCOPY SOLUTIONS' is written in white, bold, uppercase letters. The website 'edinst.com' is shown in a white box in the bottom right corner.

# Materials Research Express



## PAPER

# Investigation of the protection effect of ginger, tea tree and grapefruit essential oil extracts on mild steel in 0.5M H<sub>2</sub>SO<sub>4</sub> solution

### OPEN ACCESS

RECEIVED  
8 March 2022

REVISED  
9 June 2022

ACCEPTED FOR PUBLICATION  
13 June 2022

PUBLISHED  
22 June 2022

Roland Tolulope Loto

Department of Mechanical Engineering, Covenant University, Ota, Ogun State, Nigeria

E-mail: [tolu.loto@gmail.com](mailto:tolu.loto@gmail.com)

**Keywords:** corrosion, inhibitor, oil extracts, mild steel, H<sub>2</sub>SO<sub>4</sub>

Original content from this work may be used under the terms of the [Creative Commons Attribution 4.0 licence](https://creativecommons.org/licenses/by/4.0/).

Any further distribution of this work must maintain attribution to the author(s) and the title of the work, journal citation and DOI.



## Abstract

Utilization of plant extracts for the corrosion protection of metallic alloys has increased significantly in the last few years. Ginger (GII), tea tree (TT) and grapefruit (GP) essential oil extracts were evaluated for their corrosion protection effect on mild steel in 0.5 M H<sub>2</sub>SO<sub>4</sub> media by potentiodynamic polarization, weight loss analysis, open circuit potential measurement, optical microscopy and ATF-FTIR spectroscopy. Corrosion rate from weight loss and polarization at 0% extract concentration decreased from 63.33 mm y<sup>-1</sup> and 18.01 mm y<sup>-1</sup> to values between 0.31 mm y<sup>-1</sup> and 1.96 mm/y for weight loss, and 0.604 mm y<sup>-1</sup> and 0.161 mm/y for polarization at optimal extract concentration. Generally, the extracts performed effectively with inhibition efficiency above 95%. The extracts displayed mixed-type inhibition properties though with significant effect on the cathodic plot while the anodic plots indicate activation control mechanism. Corrosion inhibition of GII extract obeyed the Langmuir and Frumkin isotherm model while TT extract inhibition adhered to Langmuir, Frumkin, Frundlich and Temkin isotherms. GP extract inhibition obeyed the Langmuir isotherm only. Correlation coefficient of the isotherms were generally above 0.9. Adsorption of the extracts aligned with chemisorption adsorption from thermodynamic calculations. Open circuit potential plots in the presence of the extracts/acid solution generally depict significant electropositive shift compared to the plot in the absence of the extracts which was relatively electronegative. Potential variations were observed on the plots of the extracts due to miniature active passive transit characteristics at the extract-metal interphase. ATF-FTIR spectroscopic data shows the functional groups in TT extract molecules adsorbed onto the steel exterior compared to GII and GP extract molecules which depict surface coverage from analysis of the wavelength and transmittance data. Optical image of mild steel after corrosion depicts significantly degraded exterior with corrosion pits. However, in the presence of the extracts the steel morphology was well protected.

## Introduction

Degradation of carbon steels in aqueous industrial and domestic applications is of great scientific and economic importance due to the cost of maintenance of the steel in application, repair of damaged mechanical components and increasing complexity of operating environment. Carbon steel corrosion is exacerbated by the presence of multifunctional anionic species such as Cl<sup>-</sup>, SO<sub>4</sub><sup>2-</sup>, NO<sub>3</sub><sup>-</sup>, S<sub>2</sub>O<sub>3</sub>(2<sup>-</sup>) [1] within the environment. The universal applicability of carbon steels in contrast to stainless steels is due to its versatility, economic advantage, mechanical and metallurgical characteristics, ease of manufacture and recyclability [2, 3]. The application of carbon steels extends to pipeline construction, gas refining, mining, manufacture of fertilizers, radiator tank of automobiles, chemical and intermediate chemical production, energy production, heavy industrial machines, desalination plants and marine applications [4]. The high vulnerability of carbon steels to corrosion is traceable to lack of passivating elements within its microstructure, thus it is unable to produce an impenetrable protective oxide on its surface. Other factors that significantly weaken the corrosion resistance of carbon steels are the degree of moisture within the environment, pH of the environment and ionic concentration [5]. The extensive

production and application of  $\text{H}_2\text{SO}_4$  most especially as a precursor to the manufacture of other chemicals is responsible for the prevalent abundance of  $\text{SO}_4^{2-}$  anions in aqueous environments. Mining and refining of ores, processing of crude oil, production of rubber, electroplating, electrodeposition etc also involve the extensive application of  $\text{H}_2\text{SO}_4$  [6–8]. Corrosion of carbon significantly limits their operational lifespan and usefulness; hence the need for cost effect method of mitigating the corrosion problem.

Most of the conventional methods of corrosion control e.g. paint coatings, electrodeposition, hot-dip galvanization, electroplating etc are limited in versatility and cost. Corrosion inhibitors are comparatively cost effective, versatile in application and have been approved to be effective for decades in controlling corrosion. However, the known potent corrosion inhibitors in closed industrial applications are noxious, harmful to personnel and environment with regards to UN sustainable development goals e.g. arsenics, nitrates, phosphates, nitrites, chromates etc [9–11]. Corrosion inhibitors of organic origin are also toxic coupled with relatively high manufacturing cost [12–14]. Inhibitors are chemical compounds that limits the oxidation-reduction reactions liable for corrosion on metallic surfaces [15–17]. This occurs through the evolution of a protective film over the metal exterior, alteration of the corrosive medium, and adsorption on functional sites on the steel. Investigation into the corrosion protection properties of green chemical compounds with emphasis on essential oils has produced interesting results on a broad scale with some oils been effective [18–21] and others marginal in performance due to weak their adsorption properties [22–30]. Essential oils are complex aromatic compounds extracted from plant sources and majorly consist of terpenes, nitrogen, aldehydes, phenols, ketones, esters, fatty acids, alcohols, and sulphur constituents [31]. Most of the constituents are phytochemical in action with huge potential for effective protection of metallic alloys [32]. Research to establish corrosion inhibition properties of essential oil in general is ongoing and is of utmost importance due to their sustainability and availability [33–40]. Research by Znini [41], Bathily *et al* [42] and Hossain *et al* [23] reviewed a total of over 200 research publications on the corrosion inhibition properties of different essential oils. Generally, it was observed that they exhibited effective corrosion inhibition properties with respect to their concentration and chemical properties in the corrosive media coupled with mixed-type corrosion inhibition behaviour. Performance of green chemical compounds is considerably limited by weak adsorption and poor corrosion inhibition at low concentrations. This can be evaluated through adequate assessment of the corrosion protection effect of plant extracts and their minimum concentration for peak performance. This articles discusses the corrosion protection properties of ginger, tea tree and grapefruit essential oil extracts mild steel in 0.5M  $\text{H}_2\text{SO}_4$  solution.

## Experimental methods

### Materials preparation

Mild steel (MS) test pieces with circular dimension of 1.2 cm consists of 0.21% Cu, 0.29% Si, 1.04% Mn, 0.27% C, 0.08% S, 0.05% P and 98.08% Fe energy dispersive spectroscopy with PhenomWorld scanning electron microscope. The MS test pieces were cut with high speed serrating tool into separate proportion of 1 cm length for weight loss analysis. MS test pieces for potentiodynamic polarization and open circuit potential analysis were fixed to a Cu wire with soldering lead before embedded in pre-hardened epoxy mixture. The exposed surfaced of the steel was abraded with emery papers (60–1500 grits) and burnished with 6  $\mu\text{m}$  diamond solution before to washing with deionized  $\text{H}_2\text{O}$  and acetone. Ginger (GII), tea tree (TT) and grapefruit (GP) essential oil extracts were ordered from NOW Foods in the United States of America, and prepared in volumetric concentrates of 0%, 1%, 1.5%, 2%, 2.5%, 3% and 3.5% separately in 200ml of 0.5M  $\text{H}_2\text{SO}_4$  solutions.

### Potentiodynamic polarization and open circuit potential measurement

Electrochemical investigation was done at 35 °C atmospheric temperature with a Digi-Ivy 2311 potentiostat (consisting of ternary multicomponent electrode configuration within a glass beaker holding the acid-extract solution) and connected to a computer device. The electrodes are MS electrodes with visible area of 1.126  $\text{cm}^2$ , Ag/AgCl standard electrode and Pt wire counter electrode. Polarization curves were plotted at sweep rate of 0.0015  $\text{V s}^{-1}$  at potential ranges of  $-1.1 \text{ V}$  to  $+1.65 \text{ V}$ . Corrosion current density  $C_j$ , ( $\text{A cm}^{-2}$ ) and corrosion potential,  $C_p$  (V) values were obtained through Tafel derivation. Corrosion rate,  $C_{RT}$  (mm/y) was computed from the numerical expression below;

$$C_{RT} = \frac{0.00327 \times C_j \times C_q}{D} \quad (1)$$

where  $C_q$  is the equivalent weight (g) of MS, 0.00327 represents corrosion constant and  $D$  is density ( $\text{g cm}^{-3}$ ). Inhibition efficiency,  $I_{EF}$  (%) was calculated from below;

$$I_{EF} = \left[ 1 - \left( \frac{C_{RT2}}{C_{RT1}} \right) \right] \times 100 \quad (2)$$

$C_{RT1}$  and  $C_{RT2}$  represents MS weight loss without the extracts and with the extracts. Polarization resistance,  $P_R$ , ( $\Omega$ ) was computed from below;

$$P_R = 2.303 \frac{B_a B_c}{B_a + B_c} \left( \frac{1}{I_{cr}} \right) \quad (3)$$

$B_a$  and  $B_c$  represents the anodic and cathodic Tafel slopes ( $V \text{ dec}^{-1}$ ).

### ATF-FTIR Spectroscopy and Optical microscopy characterization

1% GII concentration/0.5 M  $H_2SO_4$ , 1% TT concentration/0.5 M  $H_2SO_4$  and 1% GP concentration/0.5 M  $H_2SO_4$  media before and following corrosion test were delineated under infrared particle emissions with Bruker Alpha FTIR (Fourier transform infrared spectroscopy) spectrometer limited to wavelength range of 375 to 7500  $cm^{-1}$ , and precision of 0.9  $cm^{-1}$ . Spectral patterns were analysed and matched to the standard ATF-FTIR (Attenuated total reflectance-Fourier transform infrared spectroscopy) table. Tabulations were done for the functional groups liable for the inhibition of the corrosion reaction process. Morphological image characterization of MS specimens before, and following the corrosion test in the acid media was performed with a Mustech digital microscope.

### Weight loss measurement

Weight of MS steel test pieces were computed and separately hanged in 200 ml of the acid-extract electrolyte for 240 h. Weight measurement was performed at 24 h interval. Corrosion rate,  $C_{RT}$  (mm/y) was estimated from the formulae below;

$$C_{RT} = \left[ \frac{87.6W_L}{DA t} \right] \quad (4)$$

$W_L$  illustrates weight loss (g),  $D$  is density ( $g \text{ cm}^{-3}$ ),  $A$  is total surface of the MS specimen ( $cm^2$ ) and 87.6 is the corrosion rate constant.  $t$  is time (h). Inhibition efficiency ( $\eta$ ) was computed from the following numerical relationship;

$$I_{EF} = \left[ \frac{W_{L2} - W_{L1}}{W_{L1}} \right] \times 100 \quad (5)$$

$W_{L1}$  and  $W_{L2}$  are weight loss at predetermined extract concentrations.

## Results and discussion

### Potentiodynamic polarization studies

Potentiodynamic polarization plots for MS corrosion in  $H_2SO_4$  media in the presence of specific concentrations of GII, TT and GP extracts are shown in figures 1(a)–(c). The polarization data are presented in table 1. Corrosion rate of MS at 0% extract concentration is 18.010  $mm \text{ y}^{-1}$  corresponding to corrosion current density of  $1.71 \times 10^{-3} \text{ A cm}^{-2}$  and polarization resistance of 13.31  $\Omega$ . This is confirmed from the significantly higher cathodic and anodic Tafel plots (figures 1(a)–(c)). Addition of GII, TT and GP extracts at 1% concentration substantially reduced the corrosion rate of MS to 1.751  $mm \text{ y}^{-1}$ , 0.605  $mm \text{ y}^{-1}$  and 0.480  $mm \text{ y}^{-1}$  (inhibition efficiency of 90.28%, 96.64% and 97.33%), and corrosion current density of  $1.66 \times 10^{-4} \text{ A cm}^{-2}$ ,  $5.74 \times 10^{-5} \text{ A cm}^{-2}$  and  $4.56 \times 10^{-5} \text{ A cm}^{-2}$ . Reduction in corrosion rate was observed GII extract concentration increased till 0.161  $mm \text{ y}^{-1}$  (99.11% inhibition efficiency). Corrosion rate of MS in TT/ $H_2SO_4$  solution varied with TT concentration but did not significantly decrease with corrosion rate of 0.604  $mm \text{ y}^{-1}$  (inhibition efficiency of 96.65%) at 3.5% TT concentration. MS corrosion rate increased to 0.616  $mm \text{ y}^{-1}$  at 2% GP concentration before decreasing to 0.121  $mm \text{ y}^{-1}$  (inhibition efficiency of 99.33%).

Generally, the cathodic plot for the extracts varies as extract concentration increases due to significant influence of the protonated extract molecules on the  $H_2$  evolution and  $O_2$  reduction reactions. The molecules precipitate on reactive sites on the steel surface. However, the effectiveness of the precipitation is subject to available of sufficient extract molecules. Figure 1(a) shows GII extract substantially influenced the mechanism cathodic reaction process from the substantial decrease of the cathodic portion of the polarization plot compared to TT and GP extracts. The higher the GII extract concentration, the lower the slope of the cathodic polarization plots. The anodic plots (figures 1(a)–(c)) were generally similar signifying effective surface coverage of MS through activation control and electrostatic attraction of the extract molecules. This influenced the protection effect of the extracts. Variation of corrosion potential of GII, TT and GP extract concentration to the

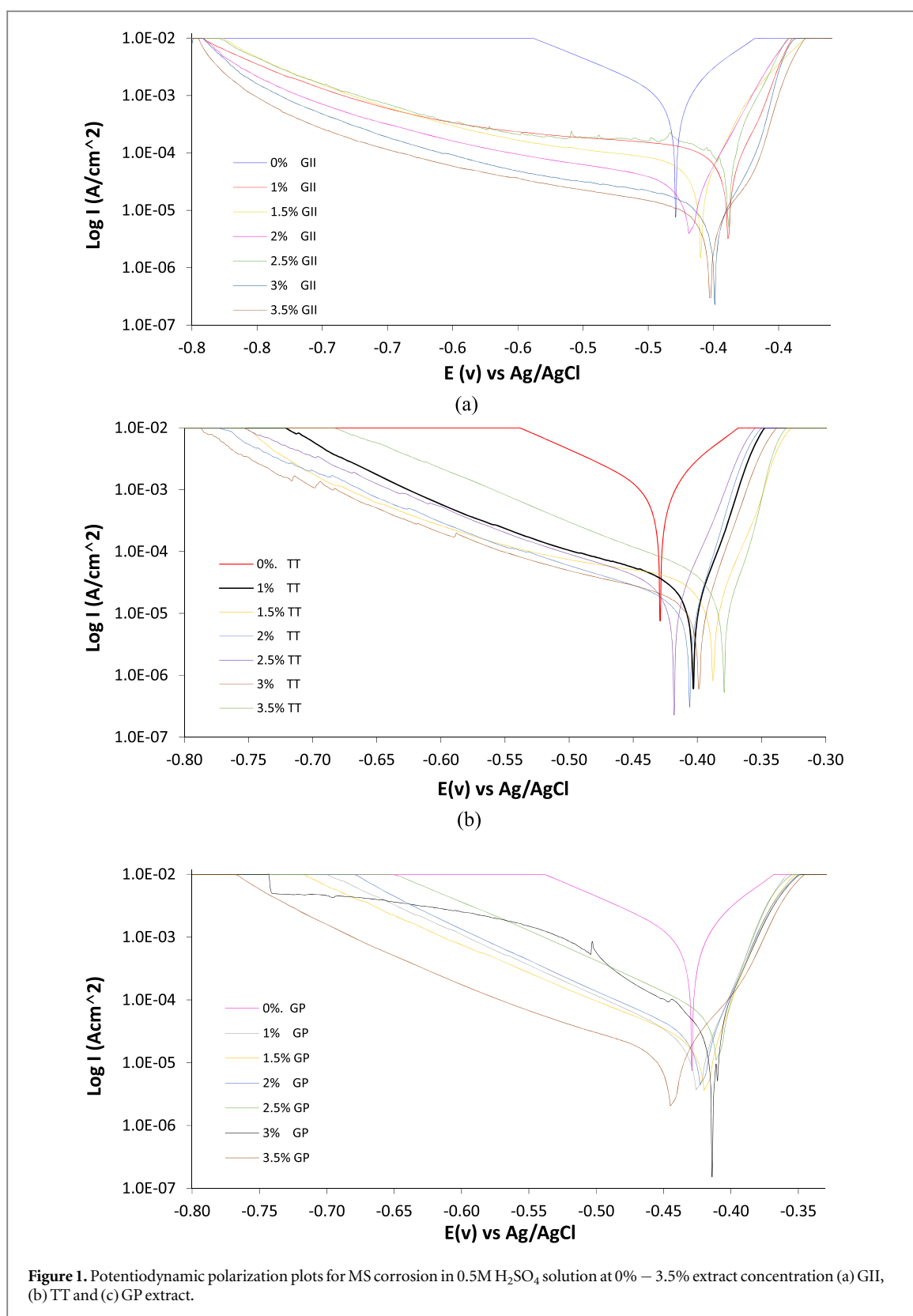


**Figure 1.** Potentiodynamic polarization plots for MS corrosion in 0.5 M  $\text{H}_2\text{SO}_4$  solution at 0% – 3.5% extract concentration (a) GII, (b) TT and (c) GP extract.

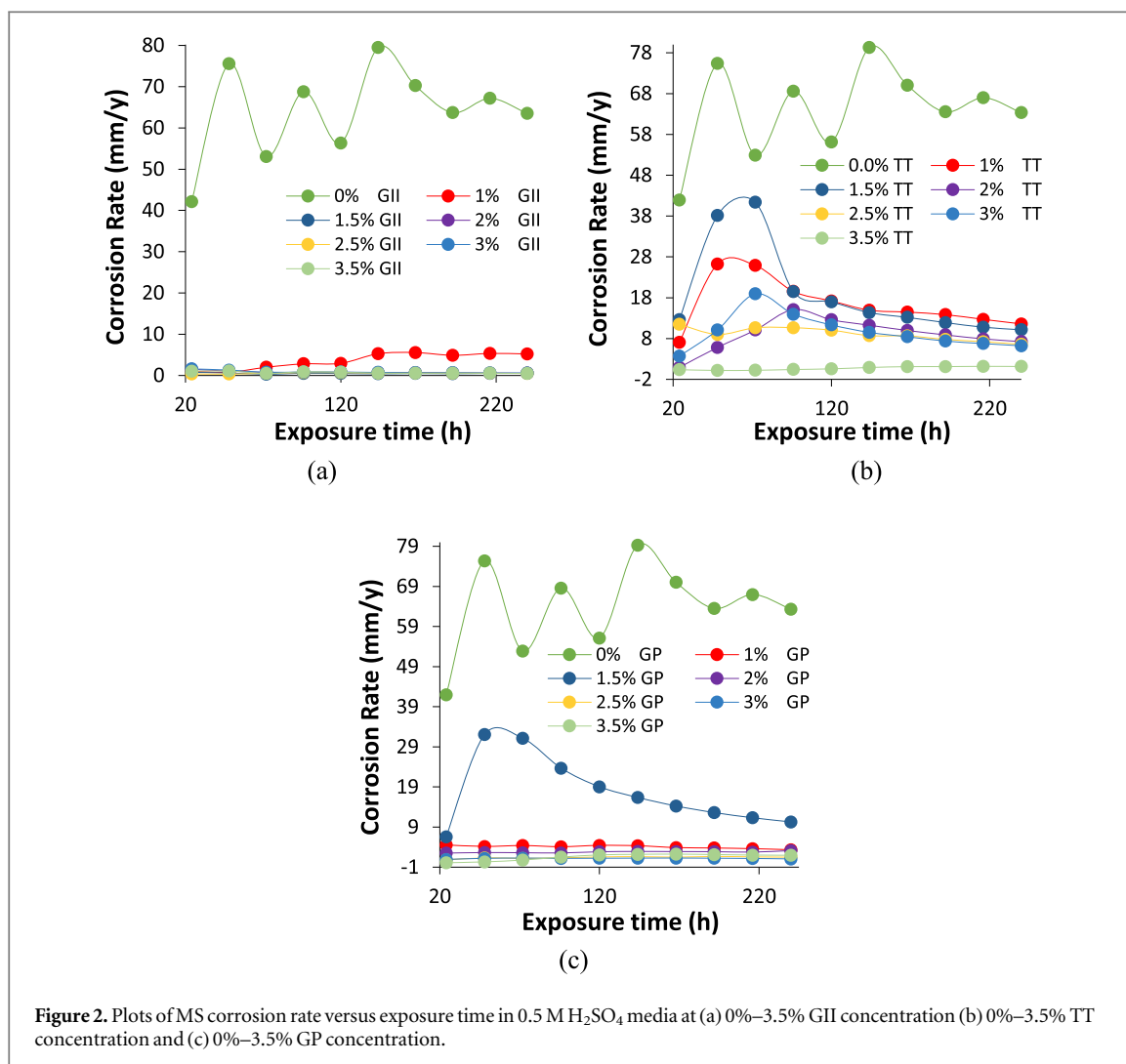
potential at 0% extract concentration shows the inhibition performance of the extracts is a mixed-type [43, 44] i.e. the extract limited the redox reaction mechanisms liable for corrosion.

#### Weight loss measurement

Comparative analysis of the corrosion inhibition effect of GII, TT and GP oil extracts on MS in 0.5 M  $\text{H}_2\text{SO}_4$  solution was performed by weight loss measurement. Plots of MS corrosion rate to measurement time in the presence of the extracts are shown from figures 2(a)–(c). Figures 3(a)–(c) shows the corresponding plots of GII,

**Table 1.** Potentiodynamic polarization data for GII, TT and GP extract inhibition on MS corrosion in 0.5M H<sub>2</sub>SO<sub>4</sub> solution.

GII extract							
Extract concentration (%)	MS corrosion rate (mm/y)	GII inhibition efficiency (%)	Corrosion current density (A cm <sup>-2</sup> )	Corrosion potential (V)	Polarization resistance, R <sub>p</sub> (Ω)	Cathodic potential, B <sub>c</sub>	Anodic potential, B <sub>a</sub>
0	18.010	—	1.71E-03	-0.429	13.31	-9.252	12.761
1	1.751	90.28	1.66E-04	-0.389	136.90	-1.813	13.792
1.5	1.095	93.92	1.04E-04	-0.410	218.80	-2.550	16.030
2	0.533	97.04	5.06E-05	-0.417	449.80	-3.404	14.250
2.5	0.402	97.77	3.82E-05	-0.388	759.54	-1.341	11.643
3	0.227	98.74	2.15E-05	-0.399	1055.00	-3.184	10.184
3.5	0.161	99.11	1.52E-05	-0.402	1492.00	-3.523	13.000
TT Extract							
Extract concentration (%)	MS corrosion rate (mm/y)	TT inhibition efficiency (%)	Corrosion current density (A/cm <sup>2</sup> )	Corrosion potential (V)	Polarization resistance, R <sub>p</sub> (Ω)	Cathodic potential, B <sub>c</sub>	Anodic potential, B <sub>a</sub>
0	18.010	—	1.71E-03	-0.429	13.31	-9.252	12.761
1	0.605	96.64	5.74E-05	-0.403	395.80	-5.462	0.742
1.5	0.486	97.30	4.61E-05	-0.388	493.20	-3.046	0.033
2	0.396	97.80	3.75E-05	-0.406	605.70	-6.174	0.048
2.5	0.586	96.75	5.56E-05	-0.418	409.00	-6.269	0.554
3	0.375	97.92	3.56E-05	-0.399	638.90	-4.704	0.020
3.5..3	0.604	96.65	5.73E-05	-0.379	397.00	-7.576	0.056
GP Extract							
Extract concentration (%)	MS corrosion rate (mm/y)	GP inhibition efficiency (%)	Corrosion current density (A/cm <sup>2</sup> )	Corrosion potential (V)	Polarization resistance, R <sub>p</sub> (Ω)	Cathodic potential, B <sub>c</sub>	Anodic potential, B <sub>a</sub>
0	18.010	—	1.71E-03	-0.429	13.31	-9.252	12.761
1	0.480	97.33	4.56E-05	-0.424	499.10	-9.625	2.15
1.5	0.520	97.11	4.93E-05	-0.418	461.10	-8.553	1.76
2	0.616	96.58	5.84E-05	-0.421	389.10	-9.409	2.71
2.5	0.180	99.00	1.71E-05	-0.409	133.00	-9.786	2.07
3	0.100	99.45	9.48E-06	-0.414	239.90	-11.926	1.15
3.5	0.121	99.33	1.15E-05	-0.435	221.00	-8.308	3.61



TT and GP inhibition efficiency values versus measurement time. Table 2 shows MS weight loss, MS corrosion rate and extracts (GII, TT and GP) inhibition efficiency data at 240 h of exposure in the electrolyte. Observation of the corrosion rate plots (figures 2(a)–(c)) shows the corrosion rate values of MS at 0% GII, TT and GP concentrations substantially varies from the plot at 1%–3.5% GII, TT and GP concentrations. This is by reason of the deteriorating action of SO<sub>4</sub><sup>2-</sup> anions in the electrolyte on MS surface through redox reaction mechanisms leading to accelerated corrosion of the steel. Corrosion rate at 0% extracts concentration initiated (24 h) at 41.95 mm y<sup>-1</sup> and progressively deteriorated to 63.33 mm y<sup>-1</sup> at 240 h. In the presence of the extracts (GII, TT and GP), the corrosion rate of the steel at all concentrations was substantially reduced. Plots in figure 1(a) shows corrosion rates of MS with GII extracts addition (1%–3.5% GII concentration) exhibited the lowest values in contrast to the plots in the presence of TT and GP extracts. In the presence of GII extract, corrosion rates initiated (24 h) at values between 0.835 and 1.392 mm/y. At 240 h, the culminating corrosion rate values varies between 0.278 and 5.012 mm/y. Corrosion rate values for TT extract varies between 1.156 and 11.582 mm y<sup>-1</sup> at 240 h while the corresponding values for GP extract varies between 1.062 mm y<sup>-1</sup> and 10.277 mm y<sup>-1</sup> respectively. It must be noted that corrosion rate of MS at 1.5% GP concentration is slightly higher than the values at 2.5% and 3% GP concentration. This observation is probably due to marginal lateral repulsion among the inhibitor molecules. The effect is marginal because the corresponding inhibition efficiency value is above 90%

Apart from 1% GII concentration, corrosion rate plots of MS were generally similar from 24 h to 240 h signifying stability of the protection effect of GII extract with reference to time and concentration. Performance of TT and GP extract visibly varies with concentration (figures 2(b) and (c)) though TT extract shows significant time dependent performance before 96 h of exposure. Further insight to the protection performance of GII, TT and GP extracts on MS in the acid electrolyte are shown from figures 3(a)–(c). GII inhibition efficiency initiated (24 h) at values between 98.01% and 99.56% (1.5% to 3.5% GII concentration) and culminated at values between 99.46% and 99.56%. Inhibition efficiency values at 1% GII concentration decreased to 92.09% at 240 h



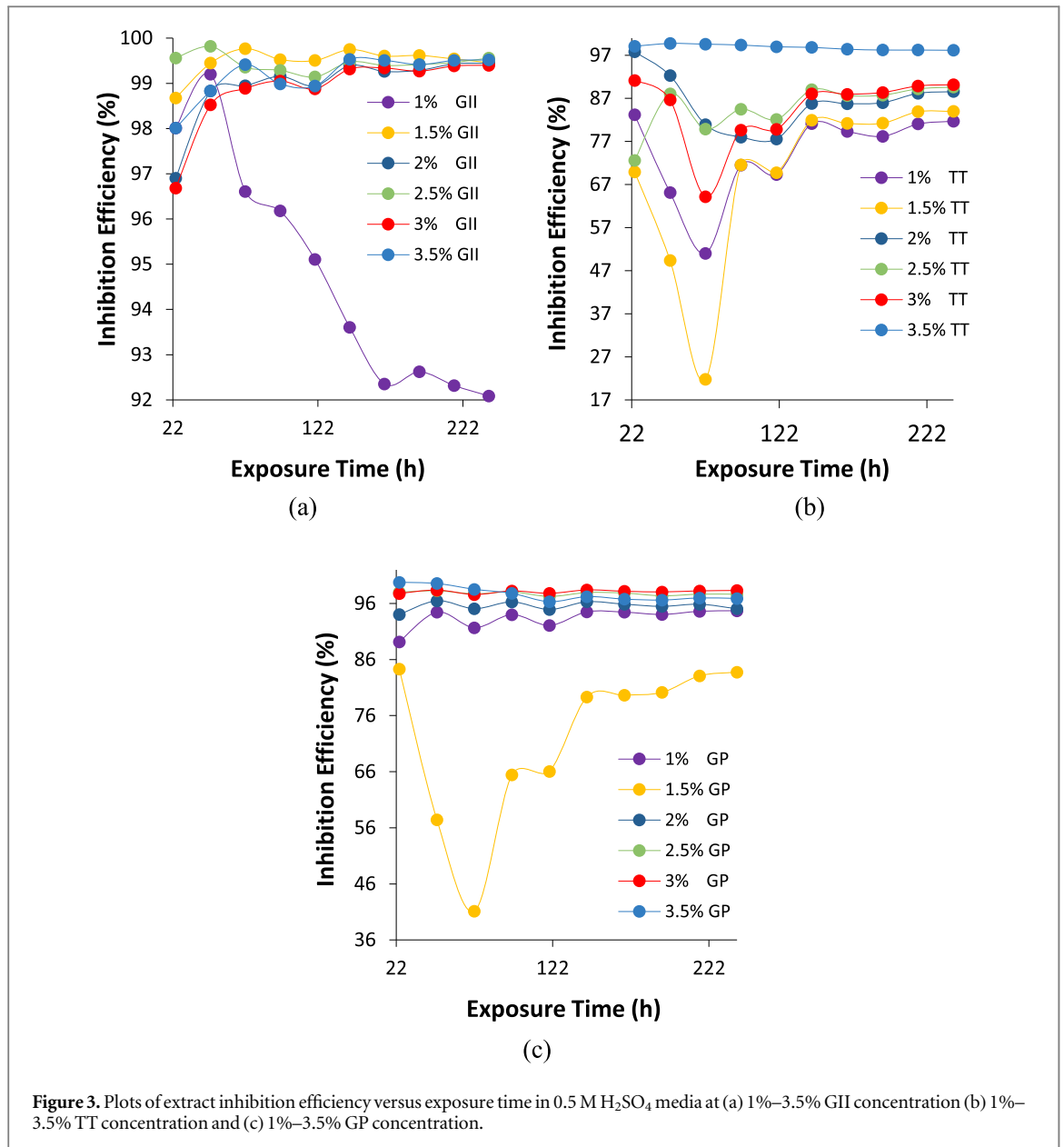


**Table 2.** Data for MS weight loss, MS corrosion rate, and extract inhibition efficiency at 240 h of exposure.

Extract conc. (%)	GII			Extract conc. (%)	TT			Extract conc. (%)	GP		
	W <sub>L</sub> (g)	C <sub>RT</sub> (mm/y)	I <sub>EF</sub> (%)		W <sub>L</sub> (g)	C <sub>RT</sub> (mm/y)	I <sub>EF</sub> (%)		W <sub>L</sub> (g)	C <sub>RT</sub> (mm/y)	I <sub>EF</sub> (%)
0%	6.823	63.33	—	0%	6.823	63.33	—	0%	6.823	63.33	—
1%	0.540	5.01	92.09	1%	1.248	11.58	81.71	1%	0.361	3.35	94.71
1.5%	0.037	0.34	99.46	1.5%	1.093	10.14	83.98	1.5%	1.107	10.28	83.77
2%	0.038	0.35	99.44	2%	0.779	7.23	88.58	2%	0.337	3.13	95.06
2.5%	0.030	0.28	99.56	2.5%	0.708	6.57	89.62	2.5%	0.160	1.49	97.65
3%	0.041	0.38	99.40	3%	0.670	6.22	90.17	3%	0.114	1.06	98.32
3.5%	0.033	0.31	99.52	3.5%	0.125	1.16	98.17	3.5%	0.211	1.96	96.91

in contrast to values at 1.5% to 3.5% GII concentration. Inhibition efficiency of TT extract generally decreased for the first 72 h before attaining relative stability at 144 h till 240 h. TT inhibition efficiency at 3.5% TT concentration was stable throughout the exposure hours. Inhibition efficiency of GP extract was stable at all concentrations but varies with concentration with the exception of 2.5% GP concentration which significantly varied with exposure time culminating at 83.77% (240 h).



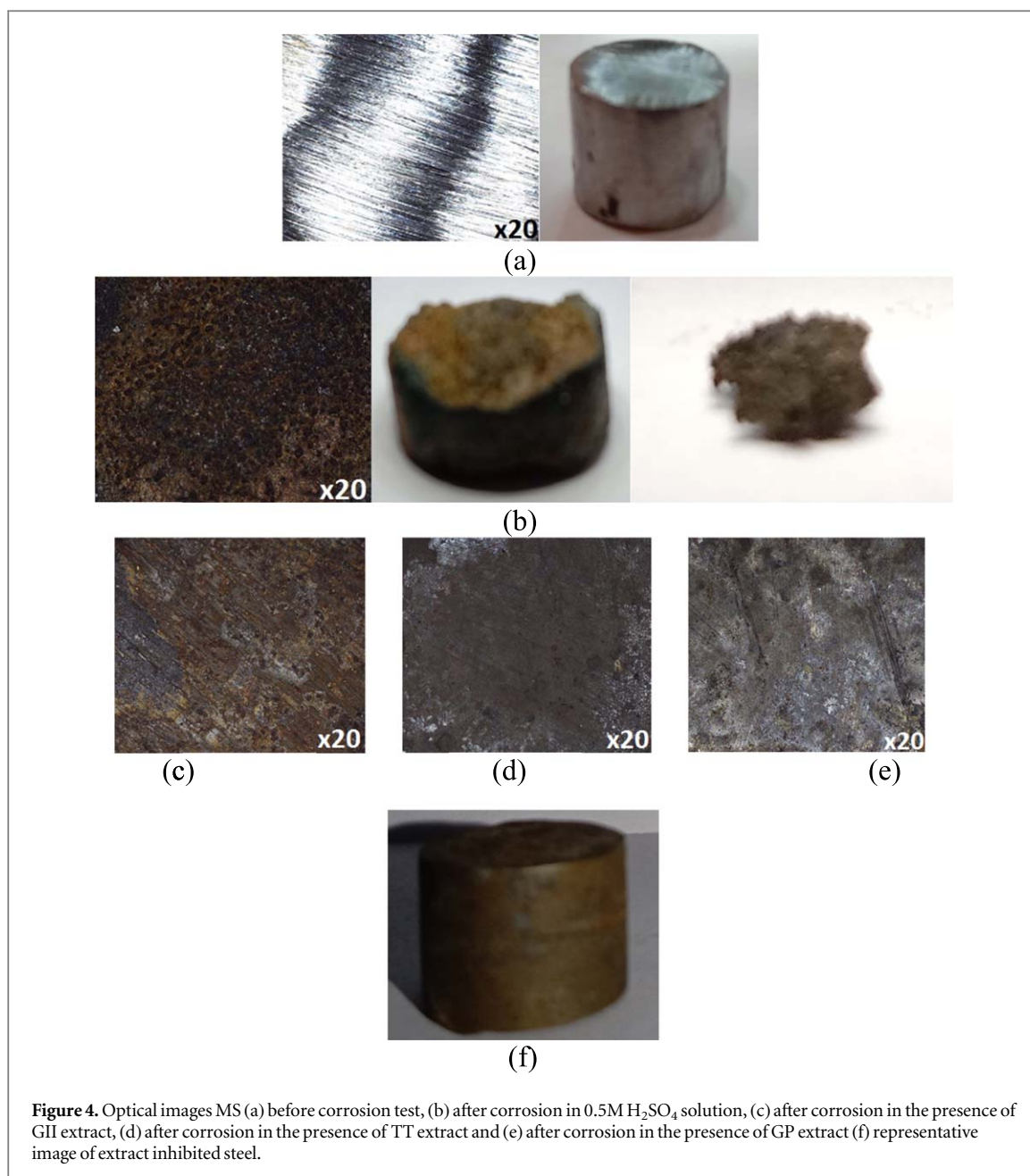


**Figure 4.** Optical images MS (a) before corrosion test, (b) after corrosion in 0.5M H<sub>2</sub>SO<sub>4</sub> solution, (c) after corrosion in the presence of GII extract, (d) after corrosion in the presence of TT extract and (e) after corrosion in the presence of GP extract (f) representative image of extract inhibited steel.

### Optical image analysis

Optical images of MS before corrosion test, after corrosion in 0.5M H<sub>2</sub>SO<sub>4</sub> solution and after corrosion in the acid electrolyte in the presence of GII, TT and GP extracts are shown from figures 4(a)–(f). The image in figure 4(b) shows severe morphological deterioration compared to figure 4(a) due to oxidation of MS surface by SO<sub>4</sub><sup>2-</sup> anions. Macro-pits are clearly visible on the surface of the steel due to displacement of ionized Fe<sup>2+</sup> anions into the electrolyte. The steel underwent accelerated corrosion and degradation in the acid solution. This image contrasts the images in figures 4(c)–(e), and figure 4(f) where the surface morphologies of MS displays sufficient resistance to electrochemical deterioration in the presence of the extracts. Morphological differences are due to the nature of electrochemical reaction between the extracts, SO<sub>4</sub><sup>2-</sup> anions and MS surface. Figure 4(c) shows GII protection involves reaction with MS surface to form non-corrosive precipitates while figures 4(d) and (e) shows the extracts forms a protective over the steel which limits the diffusion of the corrosive anions unto the steel surface.

### Adsorption isotherm and corrosion thermodynamics

Further insight into the corrosion protection effect of GII, TT and GP extracts on MS in H<sub>2</sub>SO<sub>4</sub> media was gotten from numerical equations and plots depicting the extent of differentiation of extract molecular species adsorbed

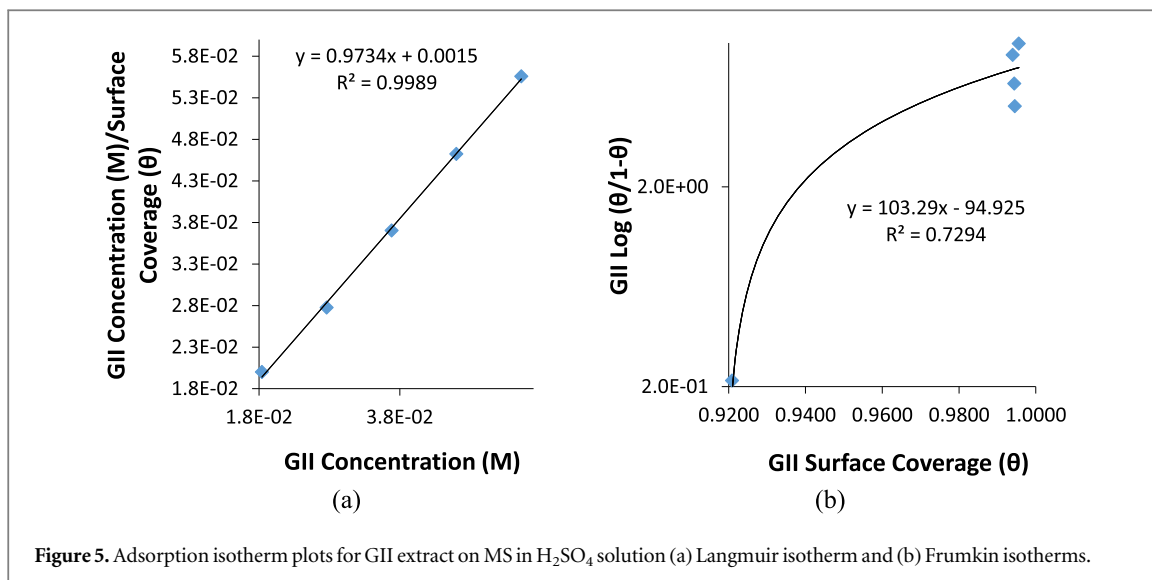


Figure 5. Adsorption isotherm plots for GII extract on MS in H<sub>2</sub>SO<sub>4</sub> solution (a) Langmuir isotherm and (b) Frumkin isotherms.

Table 3. Correlation coefficient data for relevant adsorption isotherms.

Adsorption isotherms	GII extract	GII extract	GII extract
Langmuir	0.9989	0.9994	0.9845
Frumkin	0.7294	0.9002	—
Freundlich	—	0.9037	—
Temkin	—	0.9481	—

onto the steel surface at equilibrium conditions and stable temperature [45]. Ionized molecules of the extracts transit from the aqueous phase to the metal-solution interphase during corrosion inhibition reaction processes. Data from electrochemical analysis shows the extracts influenced the anodic and cathodic plots i.e. inhibition reaction occurred through surface coverage, covalent bonding, electrostatic attraction etc Adsorption of inhibitor molecules generally involves agglomeration of inhibitor molecules from the electrolyte on the ionized metal surface. Data from weight loss experimentation were analyzed with conventional adsorption isotherms while the correlation coefficient values was applied to estimate the most relevant adsorption isotherms. Langmuir, and Frumkin isotherms gave the highest correlation coefficient values for GII extract. Langmuir, Frumkin, Freundlich and Temkin isotherms gave the highest correlation coefficient values for TT extract while Langmuir isotherms was the only relevant model for GP extract. Table 3 shows the correlation coefficient data for the relevant adsorption isotherms.

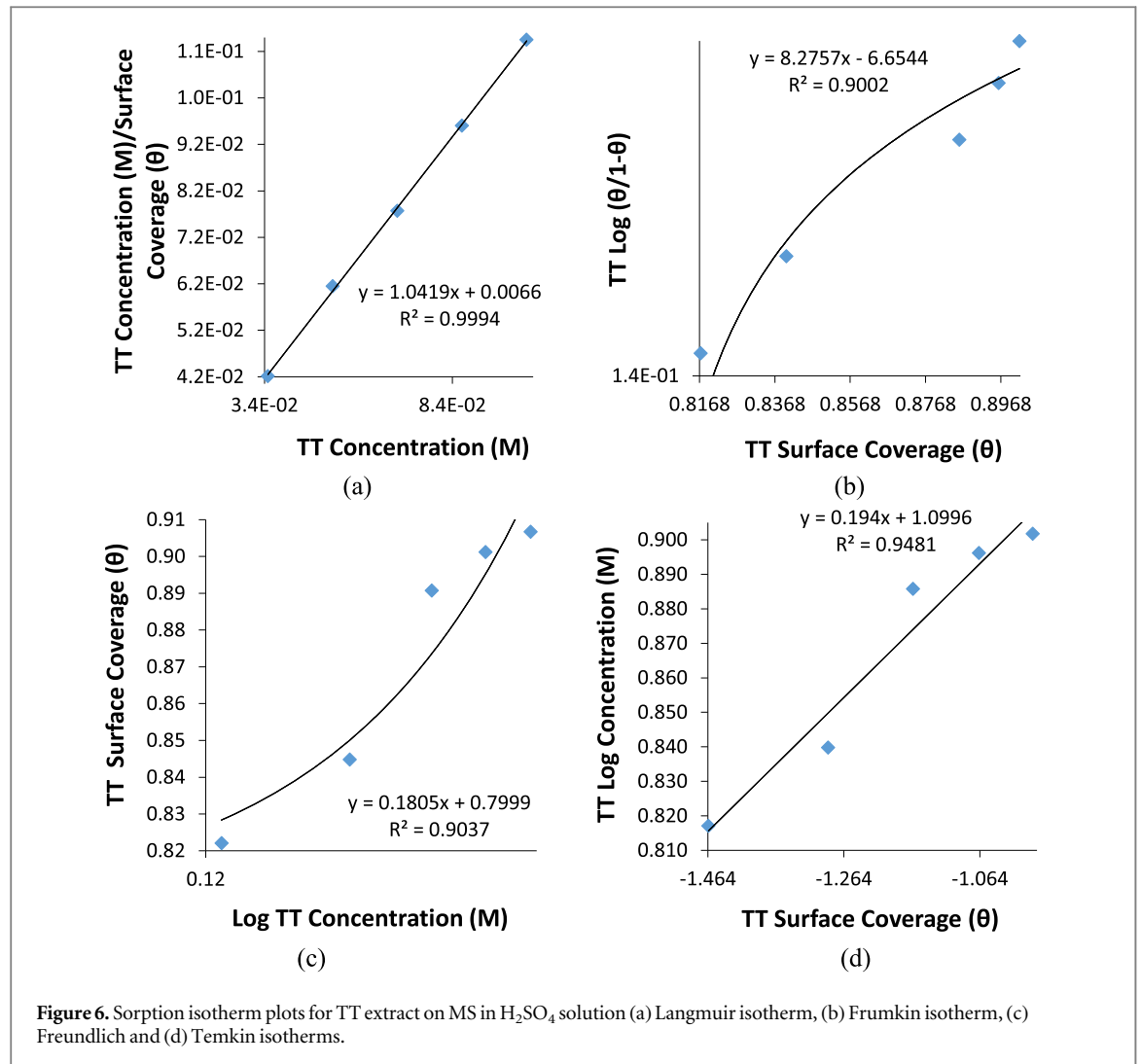
The inhibition reaction mode of GII extract on MS aligns with the Langmuir and Frumkin isotherm models. The Langmuir and Frumkin isotherm plots for GII inhibition on MS are shown in figures 5(a) and (b). Langmuir isotherm indicates that definite sum of reaction sites occurs on metallic surfaces in molecular layer form of adsorbed inhibitor molecules. The value of energy between the molecules is dependent on the dynamic equilibrium conditions in accordance with the equation below:

$$\theta = \left[ \frac{K_{ads} C_{ex}}{1 + K_{ads} C_{ex}} \right] \tag{6}$$

$K_{ads}$  represents the equilibrium constant of adsorption.  $C_{ex}$  is the molar concentration of GII, TT and GP extracts. The Frumkin isotherm indicates that molecular adsorption on ionized non-homogeneous surfaces are uniform under high concentrations with reference to the potential of the adsorbent surface. The lateral interaction effect between the extract molecules is substantial and numerical according to the equation below:

$$\log \left[ C_{TMAV} \left( \frac{\theta}{1 - \theta} \right) \right] = 2.303 \log K_{ads} + 2\alpha\theta \tag{7}$$

Langmuir, Frumkin, Freundlich and Temkin adsorption were the relevant adsorption isotherm model for TT adsorption on MS in H<sub>2</sub>SO<sub>4</sub> solution. There plots are shown in figures 6(a)–(d). The Temkin isotherm indicates that the heat of adsorption reduces in proportion to increase in surface coverage at equal binding energy distribution [46] with respect to the equation below:



$$qe = B \ln(A + C_e) \quad (8)$$

Where

$$B = \frac{RT}{b} \quad (9)$$

A represents Temkin isotherm constant (L/g), b represents Temkin constant associated with heat of adsorption, T represents temperature (K), R indicates gas constant (8.314, J/mol K) and  $C_e$  indicates concentration of adsorbate. The Freundlich isotherm indicates that adsorbed molecular interaction on metallic surfaces is related to the lateral interaction effect between them [44, 45]. The Freundlich equation is shown below:

$$\theta = KC^n \quad (10)$$

$$\log \theta = n \log C + \log K_{ads} \quad (11)$$

n represents the constant for the characteristics of adsorbed extract molecule. The Langmuir isotherm plot for GP adsorption on MS in  $H_2SO_4$  solution is shown in figure 7.

Data representing the Gibbs free energy ( $\Delta G$ ) for GII, TT and GP extracts adsorption MS surface in  $H_2SO_4$  solution are presented in table 4. The data were obtained from equation (12). Equilibrium constant of adsorption ( $K_{ads}$ ) for the extracts were obtained from Langmuir equation due to their relatively significant correlation coefficient values.

$$\Delta G_{ads} = -2.303RT \log [55.5K_{ads}] \quad (12)$$

55.5 represents molar concentration of  $H_2O$  within the electrolyte, R represents universal gas constant, T indicates absolute temperature.  $\Delta G$  data depicts chemisorption adsorption for GII, TT and GP molecules onto MS surface due to significant electrostatic effect and covalent bonding between the extract molecules and ionized MS surface [47]. The  $\Delta G$  data show  $H_2O$  molecules were substantially replaced by the extract molecules. This hinders the electrochemical action of  $SO_4^{2-}$  anions in the electrolyte. The  $\Delta G$  data for GII extract are relatively

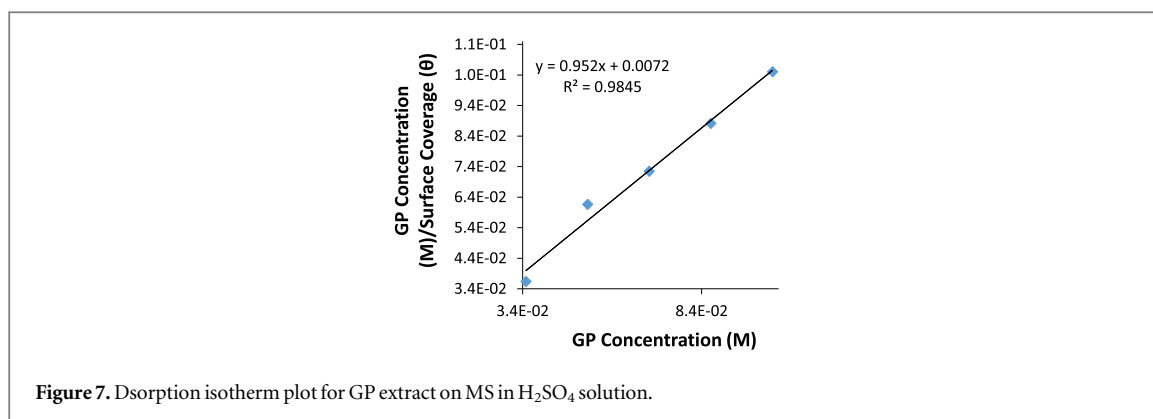


**Table 4.** Data for Gibbs free energy ( $\Delta G$ ) and equilibrium constant of adsorption ( $K_{ads}$ ) in for GII, TT and GP extract adsorption on MS in H<sub>2</sub>SO<sub>4</sub> solution.

#### GII Extract

LCS Samples	GII Concentration (Mol)	Surface Coverage ( $\theta$ )	Equilibrium Constant of adsorption ( $K_{ads}$ )	Gibbs Free Energy, $\Delta G$ ( $Kjmol^{-1}$ )
A	0	0	0	0
B	0.018	0.921	631739.27	-43.05
C	0.028	0.995	6638713.26	-48.88
D	0.037	0.994	4847293.33	-48.10
E	0.046	0.996	4917715.16	-48.13
F	0.055	0.994	2993751.33	-46.90

#### TT Extract

LCS Samples	TT Concentration (Mol)	Surface Coverage ( $\theta$ )	Equilibrium Constant of adsorption ( $K_{ads}$ )	Gibbs Free Energy, $\Delta G$ ( $Kjmol^{-1}$ )
A	0	0	0	0
B	0.034	0.817	129768.68	-39.13
C	0.052	0.840	101527.15	-38.52
D	0.069	0.886	112627.15	-38.78
E	0.086	0.896	100344.21	-38.49
F	0.103	0.902	88867.06	-38.19

#### GP Extract

LCS Samples	TT Concentration (Mol)	Surface Coverage ( $\theta$ )	Equilibrium Constant of adsorption ( $K_{ads}$ )	Gibbs Free Energy, $\Delta G$ ( $Kjmol^{-1}$ )
A	0	0	0	0
B	0.034	0.947	519991.39	-42.57
C	0.052	0.838	99965.90	-38.48
D	0.069	0.951	279197.43	-41.03
E	0.086	0.977	483579.35	-42.39
F	0.103	0.983	567832.54	-42.79

the highest values compared to other extracts due to chemisorption adsorption reaction mechanism. The lowest  $\Delta G$  data were exhibited by GP extract though the values show physiochemical interaction effect. Nevertheless, the  $\Delta G$  data for the extracts shows the molecular reaction between the extract molecules and the steel exterior stifled further corrosion of the steel surface, blocking the reaction sites and preventing electrolytic transport of  $SO_4^{2-}$  anions to the steel.

#### ATF-FTIR Spectroscopy studies

GII, TT and GP oil extracts being organic compound consists of complex molecular configuration and multifunctional organic components. Their chemisorption adsorption properties show they are non-polar and polar with high dipole moments responsible for strong electrostatic attraction and covalent bonding with MS surface. Identification of reactive groups within the complex molecules responsible for corrosion inhibition by the extracts after protonation in H<sub>2</sub>SO<sub>4</sub> media was done through ATF-FTIR spectroscopy and compared with the conventional spectroscopy table [48, 49]. The ATF-FTIR spectra plots for GII/H<sub>2</sub>SO<sub>4</sub>, TT/H<sub>2</sub>SO<sub>4</sub> and

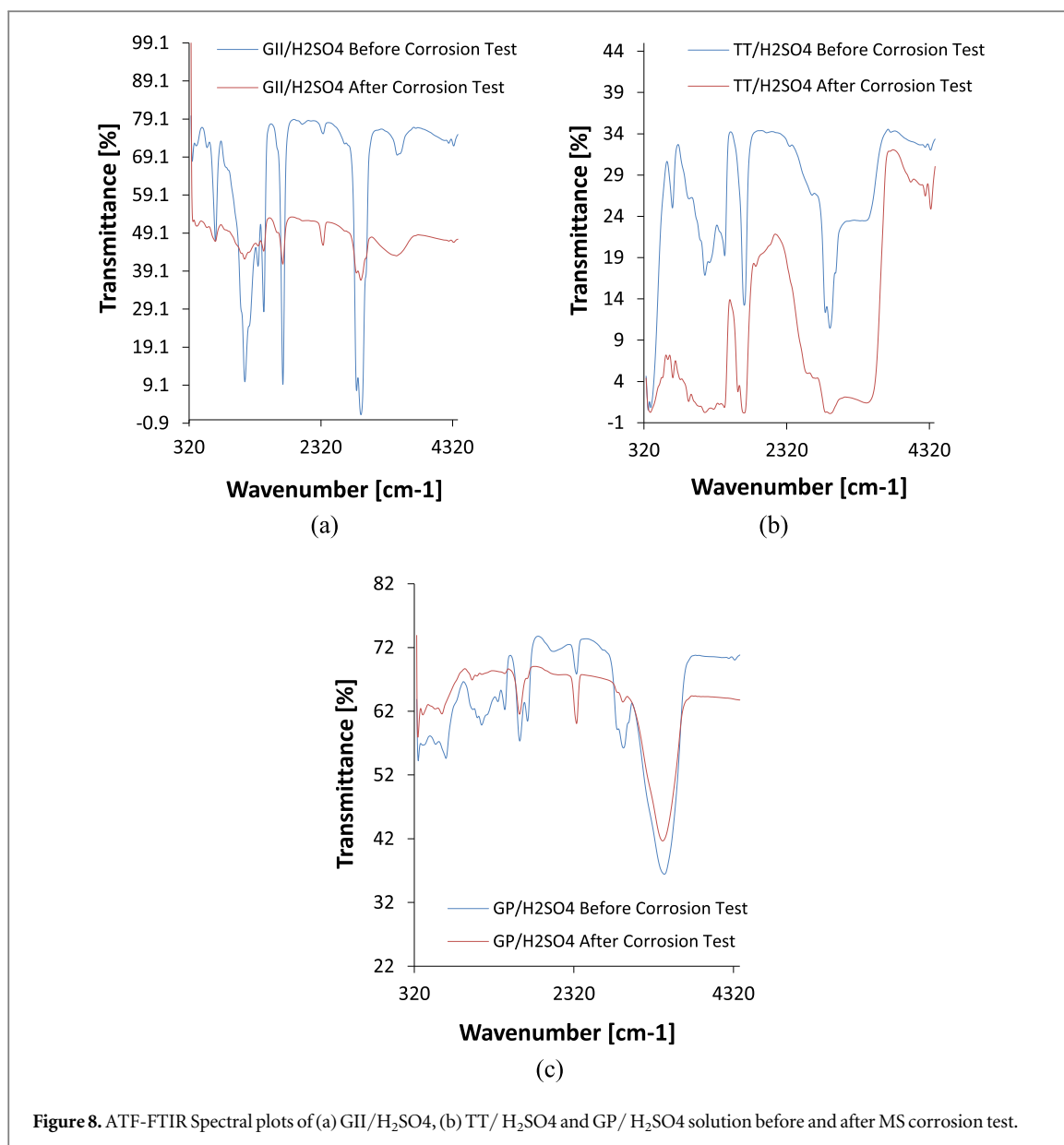


Figure 8. ATF-FTIR Spectral plots of (a) GII/H<sub>2</sub>SO<sub>4</sub>, (b) TT/H<sub>2</sub>SO<sub>4</sub> and (c) GP/H<sub>2</sub>SO<sub>4</sub> solution before and after MS corrosion test.

GP/H<sub>2</sub>SO<sub>4</sub> solutions before and following corrosion test are shown from figures 8(a)–(c). Table 5 shows the peak wavenumbers, transmittance prior to and after corrosion, the respective reactive groups and atomic bonds of the extracts in the electrolyte. The spectra plot in figure 8(b) for TT/H<sub>2</sub>SO<sub>4</sub> solution show significant decrease in transmittance for the solution after corrosion test at all wavenumbers and disappearance of the functional groups. This signifies adsorption of the reactive groups on the MS surface through chemisorption. The spectra plot in figure 8(a) shows significant increase in transmittance of the spectra peaks at specific wavenumbers where important functional groups are identified for the GII/H<sub>2</sub>SO<sub>4</sub> solution after corrosion test while at wavenumber 732 cm<sup>-1</sup>, the transmittance is the same before and after corrosion test. This assessment shows that despite the chemisorption adsorption behaviour of the extract from adsorption isotherm studies, modification of the corrosive media played a major role in limiting the diffusion of corrosive anions unto the steel surface. Within the acid solution hydrolysis of the extract results in release of the important functional groups for corrosion inhibition of the steel. Similar observation occurred for GP extract in the acid solution though at different wavenumbers.

## Conclusion

Ginger (GII), tea tree (TT) and grapefruit (GP) essential oil extracts effectively inhibited mild steel corrosion in dilute H<sub>2</sub>SO<sub>4</sub> solution at all concentrations studied. Inhibition efficiency of the extracts from weight loss measurement was between 92.09%–99.52% for GII, 81.71%–98.17% for TT and 94.71%–96.91% for GP

**Table 5.** TF-FTIR Spectroscopic table for GII/H<sub>2</sub>SO<sub>4</sub>, TT/H<sub>2</sub>SO<sub>4</sub> and GP/H<sub>2</sub>SO<sub>4</sub> solution before and after corrosion test.

<b>GII Extract</b>				
<b>Wavenumber (cm<sup>-1</sup>)</b>	<b>Transmittance (%) Before Corrosion</b>	<b>Transmittance (%) After Corrosion</b>	<b>Functional groups</b>	<b>Bonds</b>
732	47.15	47.15	alkynes, alkenes, primary and secondary amines, aromatics, alkyl alides	-C(triple bond)C-H: C-H bend, =C-H bend, O-H bend N-H wag, C-H 'oop', C-Cl stretch
1160	10.56	42.3	alcohols, carboxylic acids, esters, ethers, alkyl halids, aliphatic amines	C-O stretch, C-H wag (-CH2X), C-N stretch
1456	30.17	44.56	aromatics, alkanes	C-C stretch (in-ring), C-H bend
1748	10.8	41.03	carbonyls (general), carboxylic acids, esters, saturated aliphatic	C = O stretch
2942	2.08	36.97	carboxylic acid, alkanes	O = H stretch C = H stretch
<b>TT Extract</b>				
<b>Wavenumber (cm<sup>-1</sup>)</b>	<b>Transmittance (%) Before Corrosion</b>	<b>Transmittance (%) After Corrosion</b>	<b>Functional groups</b>	<b>Bonds</b>
724	25.14	4.45	alkynes, alkenes, primary and secondary amines, aromatics, alkyl alides	-C(triple bond)C-H: C-H bend, =C-H bend, O-H bend N-H wag, C-H 'oop', C-Cl stretch
1176	16.9	0.24	alcohols, carboxylic acids, esters, ethers, alkyl halids, aliphatic amines	C-O stretch, C-H wag (-CH2X), C-N stretch
1456	19.4	0.89	aromatics, alkanes	C-C stretch (in-ring), C-H bend
1720	13.36	0.36	carbonyls (general), carboxylic acids, aldehydes, saturated aliphatic, alpha,beta-unsaturated esters	C = O stretch
2930	10.47	0.13	carboxylic acid, alkanes	O = H stretch C = H stretch
<b>GP Extract</b>				
<b>Wavenumber (cm<sup>-1</sup>)</b>	<b>Transmittance (%) Before Corrosion</b>	<b>Transmittance (%) After Corrosion</b>	<b>Functional groups</b>	<b>Bonds</b>
676	54.78	61.74	alkenes, primary and secondary amines, aromatics, alkyl halides, alkynes, alkyl halides	=C-H bend, N-H wag, C-H 'oop', C-Cl stretch, -C(triple bond)C-H: C-H bend, C-Br stretch
1172	60.14	67.8	alcohols, carboxylic acids, esters, ethers, alkyl halids, aliphatic amines	C-O stretch, C-H wag (-CH2X), C-N stretch
1630	57.64	61.82	primary amines	N-H bend
2950	56.34	63.54	carboxylic acid, alkanes	O = H stretch C = H stretch
3458	36.44	42.01	alcohols, phenols	O-H stretch, H-bonded

extracts. The corresponding values from potentiodynamic polarization are 90.28%–99.11% for GII, 96.64%–96.65% for TT and 97.33%–99.33% for GP. The extracts significantly decreased the slope of the cathodic polarization plots with increase in concentration of the extracts in the acid solution while the anodic polarization plots were generally similar. Variation in corrosion potential was significantly minimal due to the mixed-inhibition properties of the extracts. At the lowest extract concentration, TT extract exhibited the most electropositive shift in corrosion potential relative to the plot at 0% extract concentration while at the highest extract concentration, TT and GP extracts were the most electropositive due to effective protection of the steel surface and suppression of the redox electrochemical processes. Comparison of the steel morphology from the acid solution with and without the extracts shows the extracts significantly protected the steel surface from the corrosive action of the anions in the acid solution. The wavelength and transmittance data from ATF-FTIR spectroscopy shows the active functional groups responsible for corrosion inhibitions and their possible mode of inhibition.

## Acknowledgments

The author appreciates the financial support of Covenant University towards the successful actualization of this research.

## Data availability statement

All data that support the findings of this study are included within the article (and any supplementary files).

## Declaration of interest

No conflict of interest exists.

## ORCID iDs

Roland Tolulope Loto  <https://orcid.org/0000-0002-1675-8989>

## References

- [1] Loto C A, Loto R T and Popoola A P I 2011 Corrosion and plants extracts inhibition of mild steel in HCl *Int J Phy Sci* **6** 3616–23
- [2] De Landtsheer G 2020 Design for the prevention of corrosion-under-insulation *Corrosion Under Insulation (CUI) Guidelines (European Federation of Corrosion (EFC) Series)* 3rd edn (Woodhead Publishing) ch 8 67–76
- [3] Mutahhar F, Aithan G, Iski E V, Keller M W, Shirazi S and Roberts K P 2017 Mechanistic modelling of Erosion–corrosion for carbon steel *Trends in Oil and Gas Corrosion Research and Technologies (Woodhead Publishing Series in Energy)* (Amsterdam: Elsevier B.V) (<https://doi.org/10.1016/B978-0-08-101105-8.00031-0>)
- [4] Mokhatab S, Poe W A and Mak J 2019 Raw Gas Transmission *Handbook of Natural Gas Transmission and Processing (Principles and Practices)* 4th edn (Gulf Professional Publishing) ch 3 103–76
- [5] Bobina M, Kellenberger A, Millet J P, Muntean C and Vaszilcsin N 2013 Corrosion resistance of carbon steel in weak acid solutions in the presence of l-histidine as corrosion inhibitor *Corros. Sci.* **69** 389–95
- [6] Chenier P J 1987 *Survey of Industrial Chemistry* (New York: Wiley) 45–57
- [7] Industrial Applications of Sulfuric Acid <https://worldofchemicals.com/430/chemistry-articles/industrial-applications-of-sulfuric-acid.html>
- [8] *Hydrochloric Acid, Chemicals Economics Handbook* (SRI International) 2001 4000A–3003F
- [9] Twite R L and Bierwagen G P 1998 Review of alternatives to chromate for corrosion protection of aluminum aerospace alloys *Prog. Org. Coat.* **33** 91
- [10] Bastos A C, Ferreira M G and Simões A M 2006 Corrosion Inhibition by Chromate and Phosphate Extracts for Iron Substrates Studied by EIS and SVET *Corros. Sci.* **48** 1500–12
- [11] Hernandez-Alvarado L A, Hernandez L S and Rodriguez-Reyna S L 2012 Evaluation of corrosion behavior of galvanized steel treated with conventional conversion coatings and a chromate-free organic inhibitor *Int. J. Corros.* **2012** 368130
- [12] Singh W P and Bockris J O M 1996 *Toxicity Issues of Organic Corrosion Inhibitors: Applications of QSAR Model* (Houston, TX: NACE International)
- [13] Loto R T and Olukeye T 2018 Corrosion inhibition properties of the synergistic effect of 4-hydroxy-3-methoxybenzaldehyde and hexadecyltrimethylammoniumbromide on mild steel in dilute acid solutions *J. King Saud Univ., Eng. Sci.* **30** 384–90
- [14] Solomon M M and S. A. Umoren S A 2015 Enhanced Corrosion Inhibition Effect of Polypropylene Glycol in the Presence of Iodide Ions at Mild Steel/Sulphuric Acid Interface *J. Environ. Chem. Eng.* **3** 1812–36
- [15] Gräfen H, Horn E M, Schlecker H and Schindler H 2002 Ullmann's Encyclopedia of Industrial Chemistry *Corrosion* (Weinheim: Wiley) (<https://doi.org/10.1002/14356007.b01>)
- [16] Loto R T 2017 Study of the synergistic effect of 2-methoxy-4-formylphenol and sodium molybdenum oxide on the corrosion inhibition of 3CR12 ferritic steel in dilute sulphuric acid *Results Phys* **7** 769–76



- [17] Loto R T, Joseph O O, Loto C A and Popoola A P I 2014 Corrosion inhibitive behaviour of camellia sinensis on aluminium alloy in  $H_2SO_4$  *Int. J. Electrochem. Sci.* **9** 1221–31
- [18] Sigircik G, Tüken T and Erbil M 2016 Assessment of the inhibition efficiency of 3,4-diaminobenzonitrile against the corrosion of steel *Corros. Sci.* **102** 437–45
- [19] Odiongenyi A O, Odoemelam S A and Eddy N O 2009 Corrosion Inhibition and Adsorption Properties of Ethanol Extract of *Vernonia amygdalina* for the Corrosion of Mild Steel in  $H_2SO_4$  *Port Electrochim. Acta.* **27** 33–45
- [20] Deepa Rani P and Selvaraj S 2010 *Inhibitive and adsorption properties of Punica granatum extract on brass in acid media* *J. Phytol.* **2** 58–64
- [21] Raja P B and Sethuraman M G 2008 Natural Products as Corrosion Inhibitor for Metals in Corrosive Media: A Review *Mater. Lett.* **62** 113–6
- [22] Narayanasamy P, Ramachandren T, Natesan M and Murugavel S C 2009 Corrosion Inhibition of Mild Steel by Essential Oils in an HCl Environment *Mater. Performance* **48** 52–6
- [23] Hossain S M Z, Razzak S A and Hossain M M 2020 Application of essential oils as green corrosion inhibitors *Arab. J. Sci. Eng.* **45** 7137–59
- [24] Hmamou D B, Salghi R, Zarrouk A, Zarrouk H, Errami M, Hammouti B, Afia L and Bazzi L 2013 Adsorption and corrosion inhibition of mild steel in hydrochloric acid solution by *Verbena* essential oil *Res. Chem. Intermed.* **39** 973–89
- [25] Afia L, Benali O, Salghi R, Ebenso E E, Jodeh S, Zougagh M and Hammouti B 2014 Steel corrosion inhibition by acid garlic essential oil as a green corrosion inhibitor and sorption behaviour 2014 *Int. J. Electrochem. Sci.* **9** 8392–406
- [26] Gualdrón F, Becerra E N, Peña D Y, Gutiérrez J C and Becerra H Q 2013 Inhibitory effect of *Eucalyptus* and *Lippia Alba* essential oils on the corrosion of mild steel in hydrochloric acid *J. Mater. Environ. Sci.* **4** 143–58
- [27] Bammou L, Chebli B, Salghi R, Bazzi L, Hammouti B, Mihit M and Idrissi H 2010 Thermodynamic properties of Thymus saturoioides essential oils as corrosion inhibitor of tinplate in 0.5M HCl: chemical characterization and electrochemical study *Green Chem. Lett. Rev.* **3** 173–8
- [28] Bui H T T, Dang T D, Le H T T and Hoang T T B 2019 Comparative study on corrosion inhibition of vietnam orange peel essential oil with urotropine and insight of corrosion inhibition mechanism for mild steel in hydrochloric solution *J. Electrochem. Sci. Technol.* **10** 69–81
- [29] Lahhit N, Bouyanzer A, Desjobert J M, Hammouti B, Salghi R, Costa J, Jama C, Bentiss F and L. Majidi L 2011 Fennel (*Foeniculum Vulgare*) essential oil as green corrosion inhibitor of carbon steel in hydrochloric acid solution *Port Electrochim Acta* **29** 127–38
- [30] Idouhli R, Oukhrib A, Koumya Y, Abouelfida A, Benyaich A and Benharref A 2018 Inhibitory effect of atlas cedar essential oil on the corrosion of steel in 1 M HCl *Corros. Rev.* **36** 373–84
- [31] Gro S J 2007 Post-harvest strategies to reduce enteric bacteria contamination of vegetable, nut and fruit products *Handbook of Organic Food Safety and Quality (Woodhead Publishing Series in Food Science, Technology and Nutrition)* (Woodhead Publishing) ch 20 433–53
- [32] Prakash B 2020 Functional and Preservative Properties of Phytochemicals (Amsterdam: Elsevier) (<https://doi.org/10.1016/C2018-0-03991-2>)
- [33] Fu J, Li S, Cao L, Wang Y, Yan L and Lu L 2010 Tryptophan as green corrosion inhibitor for low carbon steel in hydrochloric acid solution *J. Mater. Sci.* **45** 979–86
- [34] Bouoidina A, Chaouch M, Abdellaoui A, Lahkimi A, Hammouti B, El-Hajjaji F, Taleb M and Nahle A 2017 Essential oil of '*Foeniculum vulgare*': antioxidant and corrosion inhibitor on mild steel immersed in hydrochloric medium *Anti-Corros Method Mater* **64** 563–72
- [35] Hamdani I, El Ouariachi E, Mokhtari O, Salhi A, Chahboun N, ElMahi B, Bouyanzer A, Zarrouk A, Hammouti B and Costa J 2015 Chemical constituents and corrosion inhibition of mild steel by the essential oil of Thymus algeriensis in 1.0 M hydrochloric acid solution *Der. Pharma. Chem.* **7** 252–64
- [36] El Ouadi Y, Bouyanzer A, Majidi L, Paolini J, Desjobert J M, Costa J, Chetouani A and Hammouti B 2014 *Salvia officinalis* essential oil and the extract as greencorrosion inhibitor of mild steel in hydrochloric acid *J. Chem. Pharm. Res.* **6** 1401–16
- [37] El Ouariachi E, Bouyanzer A, Salghi R, Hammouti B, Desjobert J M, Costa J, Paolini J and Majidi L 2015 Evaluation of *Pelargonium* extract and oil as eco-friendly corrosion inhibitor for steel in acidic chloride solutions and pharmacological properties *Res. Chem. Intermed.* **41** 7125–49
- [38] Boumhara K, Tabyaoui M, Jama C and Bentiss F 2015 *Artemisia mesatlantica* essential oil as green inhibitor for carbon steel corrosion in 1 M HCl solution: Electrochemical and XPS investigations *J. Ind. Eng. Chem.* **29** 146–55
- [39] Lahhit N, Bouyanzer A, Desjobert J M, Hammouti B, Salghi R, Costa J, Jama C, Bentiss F and Majidi L 2011 Fennel (*Foeniculum vulgare*) essential oil as green corrosion inhibitor of carbon steel in hydrochloric acid solution *Port Electrochim Acta* **29** 127–38
- [40] Loto R T, Leramo R and Oyebeade B 2018 Synergistic combination effect of *Salvia officinalis* and *Lavandula officinalis* on the corrosion inhibition of low-carbon steel in the presence of  $SO_4^{2-}$  and  $Cl^-$  containing aqueous environment *J. Fail. Anal. Prev.* **18** 1429–38
- [41] Znini M 2019 Application of essential oils as green corrosion inhibitors for metals and alloys in different aggressive mediums - A review *Arabian Journal of Medicinal & Aromatic Plants.* **3** 5
- [42] Bathily M, Ngom B, Gassama D and Tamba S 2021 Review on essential oils and their corrosion-inhibiting properties *Am. J. Appl. Chem.* **9** 65–73
- [43] Lai C, Xie B, Zou L, Zheng X, Ma X and Zhu S 2017 Adsorption and corrosion inhibition of mild steel in hydrochloric acid solution by S-allyl-O'-dialkyldithiophosphates *Results in Phys.* **7** 3434–43
- [44] Al-Amiery A A, Ahmed M H O, Abdullah T A, Gaaz T S and Kadhum A M H 2018 Electrochemical studies of novel corrosion inhibitor for mild steel in 1 M hydrochloric acid *Results in Physics* **9** 978–81
- [45] Bockris J O and Swinkels D A J 1964 Adsorption of n-decylamine on solid metal electrodes *J. of Elect. Soc.* **11** 736
- [46] Lowmunkhong P, Ungtharak D and Sutthivaiyakit P 2010 Tryptamine as a corrosion inhibitor of mild steel in hydrochloric acid solution *Corros. Sci.* **52** 30–6
- [47] Loto R T 2016 Electrochemical analysis of the corrosion inhibition properties of 4-hydroxy-3-methoxybenzaldehyde on low carbon steel in dilute acid media *Cogent Eng* **3** 1242107
- [48] Philip J Y N, Buchweshaija J and Mwakalesi A 2016 *Mater. Sci. Appl.* **7** 396
- [49] Table of Characteristic IR Absorptions (<http://orgchem.colorado.edu/Spectroscopy/specttutor/irchart.pdf>) (accessed 12 January 2022)